Transmission and diffraction properties of a narrow slit in a perfect metal

B. Sturman,[1] E. Podivilov,[1] and M. Gorkunov[2]
[1]*Institute of Automation and Electrometry, Russian Academy of Sciences, 630090 Novosibirsk, Russia*
[2]*Shubnikov Institute of Crystallography, Russian Academy of Sciences, 119333 Moscow, Russia*
(Received 30 June 2010; revised manuscript received 16 August 2010; published 10 September 2010)

By solving Maxwell's equations with the perfect-metal boundary conditions in the TM case, we have fully described the transmission and diffraction properties of a single slit regardless of its width. Efficiencies of the main transformation processes—transmission, diffraction, and reflection—are analyzed in the sub-to-few-wavelength range showing a number of sharp fundamental features. These features are linked to the near-field behavior of the light fields. The transformation efficiencies are then employed to describe the Fabry-Perot resonances of perforated metal films. Close links with the case of real metals are also considered.

DOI: 10.1103/PhysRevB.82.115419 PACS number(s): 42.25.Bs, 42.25.Fx, 42.70.Qs, 73.20.Mf

I. INTRODUCTION

Solutions to electromagnetic diffraction problems based on the perfect-metal boundary conditions date back to the works of Rayleigh, Sommerfeld, and Bethe,[1–3] see also Refs. 4 and 5. Such solutions are few in number, complicated, but indispensable in the subwavelength/nano-optics where the usual Huygens-principle-based theory and intuitive approaches fail. Importantly, they link together the far- and near-field properties of the electromagnetic field including the corner singularities.[6]

The general upsurge of interest in nano-optics gave rise to many research areas involving nanostructured metals, such as near-field microscopy,[7] metal-clad cavities,[8] biosensing,[9] and extraordinary light transmission (ELT) through nanoholes.[10,11] Already the formulation of the corresponding problems strongly differs from that typical of classical optics. Instead of diffraction from plain obstacles,[4] one deals with funneling of light into (out of) apertures, with coupling of the opposite metal interfaces, with a local enhancement of the electromagnetic fields. Involvement of the surface plasmons in real metals further enriches the physics.[12]

Theoretical basis of subwavelength optics of metals is a big issue. On the one hand, direct numerical methods typically map a tiny part of the actual space of variable parameters of the system with no real insight into the physics of multiscale phenomena. On the other hand, they are capable of a dramatic enhancement of the analytical tools providing virtually exact solutions to key physical problems. Reducing complex problems to the basic elementary ones is a strong line of the studies, as it is known, e.g., for the ELT case.[13–15] The transmittance of a perforated opaque metal film can usually be accurately expressed by the efficiencies of the elementary single-interface transformation processes while the film thickness affects merely the positions of the Fabry-Perot (FP) resonances.

Here, we present a full-scale solution to the single-slit problem within the paradigm of perfect metal. This problem is among the most basic ones in nano-optics of metals. Our solution reveals a wealth of subwavelength and near-subwavelength features which have never been known. While our "perfect" problem is easier than that for real metals (owing, e.g., to the absence of the surface plasmons), it is more complicated than the Sommerfeld problem of diffraction from a single-metal wedge.[2] Furthermore, it is applicable to almost-perfect metals.

An important property of the slit geometry is the survival of a single fundamental propagating mode in the subwavelength case both for perfect and real metals. This property is inherent in any multiply connected aperture cross section,[5,16] such as, e.g., a circular slit. Our results on the single-slit transmission/diffraction properties are thus generic for a wide class of experimental geometries. Transmission and diffraction properties of single-connected apertures, such as, e.g., circular holes,[17,18] are essentially different.

A number of the previous single-slit related studies must be mentioned. Mathematical approaches to the perfect-metal single-slit case were considered early.[19] Transmission Fabry-Perot resonances for a narrow single slit in a thick perfect-metal screen have been demonstrated in connection with the ELT problem.[20,21] Phase singularities of the radiation pattern when changing the slit width were reported.[22,23] Crossover between the subwavelength regime and the geometrical-optics limit have been considered.[24] Generation of surface plasmons at a single-slit aperture have been modeled.[25,26] Transmission resonances for finite arrays of slits were analyzed.[27–29] Most of the theoretical studies employ the eigenmode-expansion method, which is adequate for the case.

Despite a big number of publications on the single-slit properties, efficiencies of the elementary processes—transmission, diffraction, and reflection—remain greatly unexplored in the sub-to-few-wavelength range for both perfect and real metals. These characteristics, which are relevant to many problems of subwavelength optics of metals, are our main concern.

II. GENERAL RELATIONS

Generally, it is necessary to consider not a single problem but two mutually related single-slit problems, "Out" and "In." They are depicted in Figs. 1(a) and 1(b). In the case Out, a plane wave of a unit amplitude and the wavelength λ is incident at the angle θ_0 from outside onto the interface $z=0$. It excites propagating modes in the slit, diffracted waves in air, and a reflected wave. In the case In, a unit-amplitude

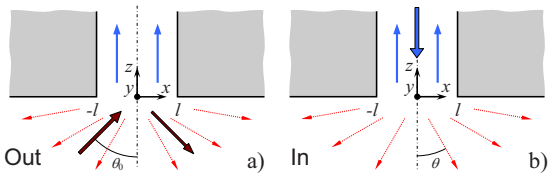

FIG. 1. (Color online) Two basic interface problems, Out and In, corresponding to the incidence from outside (a) and inside (b).

propagating mode traveling from inside to the interface $z=0$ reflects back and excites diffracted waves in air.

In the TM case in question, the magnetic field amplitude has only a y component $H=H(x,z)$, and the nonzero components of the electric field are $E_x=(-i/k_0)\partial H/\partial z$ and $E_z=(i/k_0)\partial H/\partial x$, where $k_0=2\pi/\lambda$ is the vacuum wavevector. At the air-metal boundaries, the tangential component of $\vec{E}$ and the normal component of $\vec{H}$ turn to zero.

As a full set of even and odd eigenfunctions for $z>0$, we choose[5]

$$h_\nu(x)=\begin{cases}\cos(\pi\nu x/2l), & (\nu=0,2,\ldots)\\ \sin(\pi\nu x/2l), & (\nu=1,3,\ldots),\end{cases}$$

where l is the slit half width. The corresponding eigenvalues (propagating constants) are $\beta_\nu=\sqrt{k_0^2-(\pi\nu/2l)^2}$. The real and imaginary β_ν refer to the propagating and evanescent modes, respectively. For the fundamental propagating mode, $\nu=0$, we have $\beta_0=k_0$ and $h_0(x)=1$. For $l<\lambda/4$, all other eigenmodes are evanescent.

For the case Out and $z\gtrless 0$, the field $H(x,z)$ can be represented by the general modal expansions, similar to that used successfully in the area,[19,20,24–26,29]

$$H^{>}=\sum_\nu c_\nu b_\nu h_\nu(x)e^{i\beta_\nu z},$$

$$H^{<}=2e^{ik_{0x}x}\cos(k_{0z}z)+\int_{-\infty}^{\infty}a_k e^{ikx-i\varkappa_k z}dk, \qquad (1)$$

where $k_{0x}=k_0\sin\theta_0$, $k_{0z}=k_0\cos\theta_0$, $\varkappa_k=(k_0^2-k^2)^{1/2}$, $c_0=1$, and $c_\nu=2$ for $\nu\neq 0$. For $z>0$ and $|x|\leq l$, we have satisfied Maxwell's equations and the boundary conditions at $|x|=l$. Furthermore, we have $b_\nu=\langle H^{>}(x,0)h_\nu\rangle$, where $\langle\cdots\rangle$ indicates averaging over the slit. In the air region, $z<0$, we have satisfied so far only Maxwell's equations. Here the waves with $k<k_0$ are propagating while for $k>k_0$ they are evanescent.

The amplitudes b_ν and a_k can be found if we satisfy the remaining boundary conditions: $E_x^{<}(x,0)=E_x^{>}(x,0)\Theta(l-|x|)$, where $\Theta(x)$ is the Heaviside step function, and $H^{<}(x,0)=H^{>}(x,0)$ for $|x|<l$. These conditions are equivalent to the relations

$$a_k=-\frac{l}{2\pi\varkappa_k}\sum_\nu c_\nu\beta_\nu b_\nu f_{\nu,k},$$

$$b_\nu=f_{\nu,-k_{0x}}+\frac{1}{2}\int_{-\infty}^{\infty}a_k f_{\nu,-k}dk, \qquad (2)$$

where $f_{\nu,k}=\mathrm{sinc}(kl+\pi\nu/2)+\mathrm{sinc}(kl-\pi\nu/2)$ for $\nu=0,2,\ldots$, $f_{\nu,k}=i\,\mathrm{sinc}(kl+\pi\nu/2)-i\,\mathrm{sinc}(kl-\pi\nu/2)$ for $\nu=1,3,\ldots$, and $\mathrm{sinc}(\cdots)\equiv\sin(\cdots)/(\cdots)$. For even/odd ν, the function $f_{\nu,k}$ is real/imaginary and even/odd in k. Combining Eq. (2), we come to the set of coupled-mode equations

$$b_\nu+\sum_{\nu'}T_{\nu\nu'}b_{\nu'}=f_{\nu,-k_{0x}} \qquad (3)$$

with the coupling coefficients

$$T_{\nu\nu'}=\frac{l}{4\pi}\beta_{\nu'}c_{\nu'}\int_{-\infty}^{\infty}\frac{f_{\nu,-k}f_{\nu',k}}{\varkappa_k}dk. \qquad (4)$$

Obviously, $T_{\nu\nu'}=0$ for the modes of different parity, i.e., the set (3) splits into two sets—for the even and odd modes. Calculating b_ν from Eq. (3) and using Eq. (2) for a_k, we solve *completely* the problem Out. In the case of normal incidence, $\theta_0=0$, the amplitudes b_ν are nonzero only for the even modes and the driving force in the right-hand side of Eq. (3) is $f_{\nu,0}=2\delta_{\nu 0}$.

Using Eqs. (1) and (2) and the integral representations[30] for the Hankel function $H_0^{(1)}$, one can prove lastly an important integral relation for the diffracted component of $H^{<}$,

$$H_d^{<}=-\frac{k_0}{2}\int_{-l}^{l}E_x^{>}(x',0)H_0^{(1)}(k_0\sqrt{(x-x')^2+z^2})dx'. \qquad (5)$$

It generalizes the Huygens principle. The $H_0^{(1)}$ function describes a point irradiation source placed at $z'=0$ while the field $E_x^{>}(x',0)$, which is nonzero only for $|x'|<l$, serves as an effective density of the oscillating magnetic moment. The effective distributed irradiation source replaces indeed the real source—the surface currents at the air-metal boundaries.

The problem In can be treated similarly. In the subwavelength case, which is of our prime interest, the propagating mode incident from the inside is fundamental. Repeating the calculations, we come to the following simple symmetry relations for the amplitudes of the excited waves/modes:

$$a_k^{in}=-a_k,\quad b_0^{in}=1-b_0,\quad b_\nu^{in}=-b_\nu\ (\nu\neq 0), \qquad (6)$$

where the amplitudes a_k and b_ν, corresponding to the case Out, are taken for the normal incidence, $\theta_0=0$. Thus, the description of the problem In is reduced to that of the problem Out.

III. MODE AMPLITUDES

Computation of the coupling coefficients $T_{\nu\nu'}$ and determination of the amplitudes b_ν via truncation of Eq. (3) present no special problems, see also below. At the same time, the fundamental limit $l\to 0$ can be treated analytically. We have here $T_{00}\to 0$, $f_{\nu,-k_{0x}}\to 2\delta_{\nu 0}$, and, correspondingly, $b_0\equiv\langle H^{>}(x,0)\rangle\to 2$ for any θ_0. Furthermore, we have $b_\nu\to 0$ for $\nu\neq 0$. Similar observations are known in the literature.[19,25]

The dependence of the amplitudes b_ν on the angle of in-

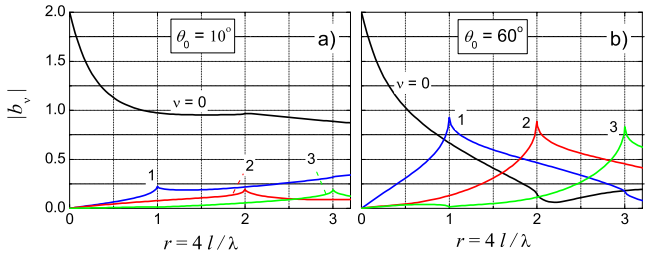

FIG. 2. (Color online) The amplitudes $|b_{0,1,2,3}|$ versus $4l/\lambda$ for $\theta_0=10°$ (a) and 60° (b). For the chosen truncation number, $\nu_{\max}=20$, the numerical error is within the line thickness.

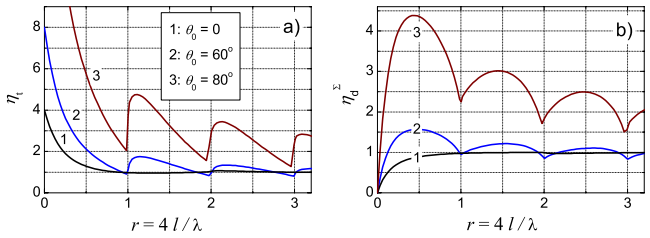

FIG. 3. (Color online) (a) The transmission efficiency and (b) the total diffraction efficiency versus $r=4l/\lambda$ for $\theta_0=0$, 60°, and 80°.

cidence θ_0 and on the characteristic ratio $r=4l/\lambda$ exhibits *clearly pronounced peculiarities*. The cases of small and large angle of incidence are essentially different, see Fig. 2. For $\theta_0 \lesssim 10°$, the situation is close to that for $\theta_0=0$. The fundamental zero mode dominates everywhere, the function $|b_0|(r)$ drops first from 2 to $\simeq 1$ and remains then almost constant while $|b_{1,2,\ldots}|(r) \ll 1$.

For $\theta_0 \gtrsim 30°$, the zero mode dominates only for $r \lesssim 0.5$. Otherwise, there is a strong mode competition. The opening of new propagating modes at $r \equiv 4l/\lambda = 1,2,\ldots$ is linked to sharp peaks of $|b_{1,2,\ldots}|(r)$. The odd and even peaks are comparable with each other tending to 1 for $\theta_0 \to 90°$. Mutual influence only of the eigenmodes of the same parity is also evident. Furthermore, only a few nearest modes dominate for each particular value of r, i.e., a *selective mode excitation* takes place.

IV. INTERFACE CHARACTERISTICS

Consider now the interface characteristics. For the problem Out, the transmission properties can be described by the efficiency

$$\eta_t(r,\theta_0) = \sum_\nu c_\nu |b_\nu|^2 \,\mathrm{Re}\, \beta_\nu/k_0 \cos\theta_0, \tag{7}$$

which is the ratio of the energy flux through the slit to the flux incident onto the slit. Obviously, the transmission efficiency is the sum of the partial contributions from all present propagating modes. For $r \equiv 4l/\lambda \leq 1$ we have $\eta_t(r,\theta_0) = |b_0|^2/\cos\theta_0$; this gives $\eta_t(0,\theta_0) = 4/\cos\theta_0$ for $r \to 0$.

Similarly, we introduce the differential diffraction efficiency for the problem Out,

$$\eta_d(r,\theta,\theta_0) = \pi k_0 \cos^2\theta |a_k|^2/l \cos\theta_0, \tag{8}$$

where $\theta = \arcsin(k/k_0)$ is the diffraction angle, see also Fig. 1(a). Owing to the symmetry relations (6), we obtain immediately for the problem In,

$$\eta_d^{in}(r,\theta) = \eta_d(r,\theta,0). \tag{9}$$

Integrating $\eta_d(r,\theta,\theta_0)$ over θ, we obtain the total diffraction efficiency for the problem Out, $\eta_d^\Sigma(r,\theta_0)$. Similarly, one can calculate the total diffraction efficiency for the problem In. The products $2l\cos\theta_0\eta_{t,d}$ give the cross sections of the corresponding elementary transformation processes. Lastly, the difference

$$R_{in}(r) = 1 - \eta_d^\Sigma(r,0) \tag{10}$$

gives the internal-reflection coefficient for the problem In, see also Fig. 1(b). In the limit $r \to 0$, we have $\eta_d^\Sigma(0,\theta_0)=0$ and $R_{in}(0)=1$.

Owing to the nondissipative character of the transformation processes in the perfect metal, the amplitudes b_ν obey the energy conservation law, which is similar to the "optical theorem" of the scattering theory.[16] It looks especially simple and useful for the normal incidence: $\eta_t + \eta_d^\Sigma = 2\,\mathrm{Re}\, b_0$. In particular, this relation enables one to express the argument (phase) of b_0 by η_t and η_d^Σ for $r<2$.

Concerning the truncation procedure, it is sufficient to take into account 1–3 evanescent modes in addition to the propagation modes in order to achieve a subpercent accuracy for $\eta_{t,d}$ and to fulfill nicely the energy conservation law. This means that $\nu_{\max} \approx [4l/\lambda]+3$. Since increasing ν_{max} presents no numerical problems, we use $\nu_{max}=20$ in this section. The numerical error is within the line thickness in the whole range of r in this case.

Figure 3 shows the behavior of η_t and η_d^Σ when changing $r=4l/\lambda$ and θ_0. It should be considered in cojunction with Fig. 2. With $\eta_t(0)=4/\cos\theta_0$, the function $\eta_t(r)$ is decreasing up to $r=1$. Further increase in r results in bursts at the openings of new propagating modes. For $\theta_0=0$, small bursts occur only at $r \simeq 2,4,\ldots$ With increasing θ_0, they appear also at $r \simeq 1,3,\ldots$ and become all highly pronounced and asymmetric. The asymmetry is due to a sharp square-root-law growth of the propagating constants $\beta_\nu(r)$ for $r > \nu$. The function $\eta_d^\Sigma(r)$ grows initially with a θ_0-dependent slope. The further scenario depends on the angle of incidence θ_0. For $\theta_0 \ll 1$, one sees only small bursts. Correspondingly, the reflection coefficient R_{in} decreases from 1 to almost 0 with increasing r. For large θ_0, the first maximum of $\eta_d^\Sigma(r,\theta_0)$, situated deeply in the subwavelength range, considerably exceeds 1, and the subsequent oscillations are highly pronounced and almost symmetric. Sharp minima of $\eta_d^\Sigma(r)$ occur at zeros of $\beta_\nu(r)$, i.e., at the sharp maxima of $|b_\nu|(r)$ in Fig. 2(b).

Figure 4 shows what happens to $\eta_d(\theta)$ when increasing r and θ_0. For $\theta_0=0$, the quasi-isotropic distribution $\eta_d(\theta) \simeq$ const, which occurs for $r \lesssim 1$, transforms gradually into a central peak growing and narrowing for $r \gg 1$. After the opening of the second even propagating mode ($r>2$) this peak acquires oscillating tails. For sufficiently large positive values of θ_0, the main difference in the behavior is in a progressive shift of the peak to the right with increasing r.

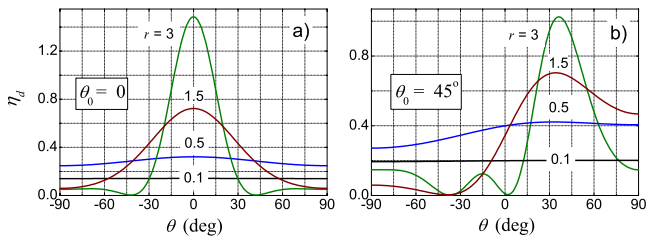

FIG. 4. (Color online) The differential diffraction efficiency for (a) $\theta_0=0$ and (b) 45°. The curves refer to $r=0.1$, 0.5, 1.5, and 3.

For $r \gg 1$, the value of θ_{peak} approaches θ_0 and the diffracted waves concentrate around the reflected one.

As seen from Fig. 4, the differential diffraction efficiency $\eta_d(r,\theta,\theta_0)$ remains nonzero for $\theta \to \pm 90°$, i.e., for ultimately large diffraction angles. This "grazing diffraction" grows remarkably and becomes strongly asymmetric with increasing θ_0: $\eta_d(90°) \gg \eta_d(-90°)$. As a function of r, $\eta_d(\pm 90°)$ experiences oscillations which correlate to those of $\eta_d^{\Sigma}(r)$. Importantly, the "grazing" diffraction is closely related to the excitation of the surface plasmons in real metals, see also below.

V. FABRY-PEROT RESONANCES

The interface characteristics considered are sufficient to describe the transmission and diffraction properties of a subwavelength slit in a metal film of a thickness d.[13,15] To illustrate it, we consider the case of normal incidence, $\theta_0=0$. Internal reflections of the fundamental propagating mode from the opposite interfaces lead to a sequence of the FP resonances. The in-slit intensity of the propagating mode is trivially given by

$$|b_0(d)|^2 = \frac{\eta_t}{|1 - R_{in} \exp[2i(\beta_0 d + \varphi_{in})]|^2}, \qquad (11)$$

where $\beta_0=k_0$ and the phase $\varphi_{in}=\arg(b_0^{in})$ is expressible by $\eta_t(r)$ and $\eta_d^{\Sigma}(r,0)$ according to the formulas of Sec. IV.

The positions of the transmission resonances are given by $k_0 d+\varphi_{in}=\pi, 2\pi, \ldots$. Figure 5(a) shows the corresponding resonant values of d/λ as functions of $r \equiv 4l/\lambda$. Adjustment to the FP resonance presents no special problems. The minimum resonant thickness, $(d/\lambda)_{\min} \simeq 0.2$, can be realized at $r \approx 1.44$.

Two quantities are of particular interest. First, it is the resonant intensity enhancement factor $\xi_{in}=|b_0^+(d)|^2_{\max}$, which

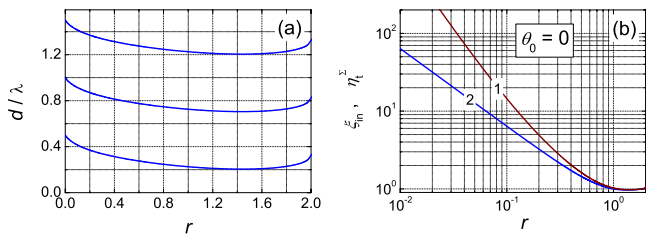

FIG. 5. (Color online) (a) A few lowest FP transmission resonances. (b) The resonant in-cavity enhancement factor ξ_{in} (curve 1) and the total-transmission efficiency η_t^{Σ} (curve 2) versus $r \equiv 4l/\lambda$.

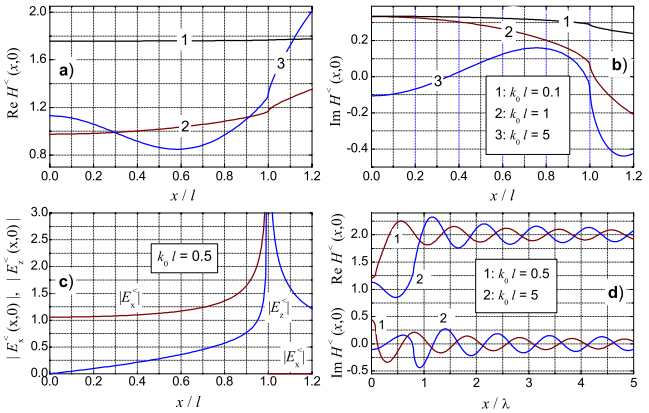

FIG. 6. (Color online) Dependences $H^<(x,0)$ and $E^<_{x,z}(x,0)$ in the near and far fields. Curves 1, 2, and 3 in the cases (a) and (b) are plotted for $k_0 l=0.1$, 1, and 5. Curves 1 and 2 in (c) correspond to $k_0 l=0.5$. The far-field profiles 1 and 2 in (d) correspond to $k_0 l=0.5$ and 5.

is the maximum (in d/λ) ratio of the in-slit intensity to the intensity of the incident wave. Second, it is the resonant total-transmission efficiency through the film η_t^{Σ}, which is the maximum ratio of the outgoing energy flux to the flux incident onto the slit. These resonant quantities are given by

$$\xi_{in} = \frac{\eta_t}{(1-R_{in})^2}, \quad \eta_t^{\Sigma} = \frac{\eta_t}{(1-R_{in})}. \qquad (12)$$

The factor $1-R_{in}$, entering Eq. (12), represents the reflection losses at each interface; it can be calculated using Eq. (10). Both ξ_{in} and η_t^{Σ} grow rapidly with decreasing r, as shown in Fig. 5(b). The angular distribution of light behind the film is given by $\eta_d(r,\theta,0)$, see Fig. 4(a).

It is worthy of mentioning that the resonant transmission cross section $2l\eta_t/(1-R_{in})$ tends to $\lambda/2$ for $r \to 0$. This asymptotic behavior follows from the single-mode model where $\eta_t \simeq 4$ and $\eta_d^{\Sigma} \equiv 1-R_{in} \simeq 4r$ for $\theta_0=0$ and $r \ll 1$. This behavior is also supported by our numerical calculations. Last, it is in agreement with dimensional considerations: The only nonzero length parameter in our disposal is λ.

VI. NEAR-FIELD PROPERTIES

In addition to the above transformation efficiencies, the spatial profiles $H^<(x,0)$ and $E^<_{x,z}(x,0)$ show intimate features of the subwavelength behavior. Figure 6 shows these profiles for the normal incidence, a few representative values of the product $k_0 l$, and $\nu_{\max}=200$. So high value of the truncation number is needed solely to resolve the corner singularities at $|x|=l$; it is excessive for the transformation efficiencies. This means that the modal expansions for $H^>(x,0)$ and $E^>_{x,z}(x,0)$ converge slowly at $x \simeq \pm l$ while the first averages $\langle H^>(x,0) h_{0,1,2}(x) \rangle$ converge quickly with increasing ν_{max}.

The profile $H^<(x,0)$, see Figs. 6(a) and 6(b), consists of two distinct sections (inside and outside the slit) separated by the inflection points at $|x|=l$. In the subwavelength range, the function $H^<(x,0)$ is structureless inside the slit and tending to the limiting value $H(\infty,0)=2$ for $k_0 l \to 0$, which corre-

sponds to the slitless case. The same limiting value takes place for $\theta_0 \neq 0$. This is why we have $b_0 = \langle H^>(x,0)\rangle \to 2$ and $\eta_t \to 4/\cos\theta_0$ for $k_0 l \to 0$. For $k_0 l \sim 1$, we have already $H^<(x,0) \simeq 1$, which corresponds to a weakly perturbed entering into the slit and to $\eta_t \approx 1$, see Fig. 3(a). For $k_0 l = 5$, the corner value $H^<(l,0)$ is close to 4/3, which corresponds to the Sommerfeld solution for a single-metal wedge.[2] Larger values of $H^<(l,0)$ for $k_0 l \lesssim 1$ are due to the mutual influence of the wedges.

Figure 6(c) shows the near-field behavior of $E_x^<(x,0)$ and $E_z^<(x,0)$. The first function, serving as an effective distributed radiation source in Eq. (5), is even in x and zero valued for $|x| > l$. For $l > \lambda$, i.e., after opening of the second propagation mode, it acquires an internal substructure. The second function, which is odd in x, is not restricted to the slit area $|x| < l$. At the inflection points, both functions tend to infinity approximately as $|x-l|^{-1/3}$, which corresponds to the 90° corner singularities of the perfect metal.[5,6] The larger $\nu_{\max}$, the better is resolved the singular behavior.

Figure 6(d) illustrates the far-field behavior which corresponds to formation of the grazing diffracted waves. Far from the slit, where the characteristic spatial scale is λ, we see a quickly establishing radiation pattern superimposed on the background value $H^<(\infty,0) = 2$. The "grazing-wave intensity" $|H^<(x,0) - 2|^2$ decreases as $1/|x|$ without oscillations for $x - l \gtrsim \lambda$, as expected for the two-dimensional case. As a function of $k_0 l$, it grows and then oscillates. A similar feature of $\eta_d(\pm 90°)$ has been mentioned in Sec. IV. The grazing-intensity oscillations, which occur for $l > \lambda$, are of the interference origin. In accordance with Eq. (5), they are controlled by the structure of the distributed effective radiation source $E_x^<(x,0)$. In particular, the grazing-wave intensities are not much different for $k_0 l = 0.5$ and 5.

VII. DISCUSSION

Our results show that the growth of the transmission efficiency $\eta_t(r,\theta_0)$ for $r \equiv 4l/\lambda \to 0$ and $\theta_0 \to \pi/2$ is directly linked with the general feature of the near-field behavior: The average over the slit $\langle H(x,0)\rangle$ tends to 2 (the slitless limit) for $r \to 0$ leading to the amplitude of the propagating mode $b_0 = 2$ for any θ_0.

The presence of noticeable grazing diffraction, see Figs. 4 and 6(d), elucidates the mechanism of surface-plasmon generation in real metals. The radiation mechanism, pertaining near the slit, is almost the same for the perfect metal and for real metals with large negative values of the optical permittivity ε_m. The presence of the localized surface mode in the latter allows to catch the waves diffracted at large angles. The surface-plasmon excitation efficiency can be evaluated as $\eta_{sp} \simeq N \eta_d(\pi/2)$, where $N = 2/\sqrt{|\varepsilon_m|}$ is the numerical aperture. This simple estimate is in good agreement with the calculations of Refs. 25 and 26.

The predicted strong resonant enhancement of the in-slit intensity in the subwavelength range, see Fig. 5(b), can be of practical interest. First, it can be useful for implementation of nonlinear-optical effects when filing the slit with a transparent nonlinear material. Second, it can be interesting for realizing sensitive nanosensors of single molecules, including biosensors.

Under certain restrictions, the perfect-metal model can be applicable to real metals. The efficiencies η_t and η_d^Σ and the reflection coefficient R_{in} should not experience strong changes for $k_0 l > |\varepsilon_m|^{-1/2}$, when the slit width exceeds the skin depth and $\beta_0 \simeq k_0$.[31,32] In many cases $|\varepsilon_m| \gtrsim 10^2$,[33] and the above restriction on $k_0 l$ is rather soft. For $l/\lambda \to 0$, the single-interface characteristics, especially η_t, can experience substantial changes. The main impact of the metal imperfection on the FP resonances comes from the inequality $\beta_0 \neq k_0$, see Eq. (11), i.e., from competition between the bulk and interface losses and displacement of the resonant values of d/λ.

The single-slit near- and far-field properties, see Fig. 6, elucidate the mechanism of coupling of neighboring slits in multislit systems.[14,27–29] This coupling occurs indeed via the secondary scattering of the grazing waves and must be strongly dependent on the slit width and the slit separation. In real metals, it should compete with the surface-plasmon coupling mechanism possessing essentially different characteristics.

The corner singularities are clearly seen in the near field for $\nu_{\max} \gtrsim 10^2$. However, they are uncoupled from the diffraction/transmission properties. The latter are linked to several lowest modes, i.e., to rough features of the near-field behavior. A small-radius edge rounding is thus not expected to produce a strong effect on $\eta_{t,d}$.

Being relatively simple and compact, our perfect-metal related results can be considered as a reference point in subwavelength optics of real metals where the wealth of possibilities creates serious computational and perceptual problems.

VIII. CONCLUSIONS

In conclusion, a full-scale physical picture of the transmission, diffraction, and near-field properties of a single slit in the perfect metal is presented. In the sub-to-near-subwavelength range, the transformation efficiencies show sharp dependences on l/λ and θ_0 which are closely linked to the near-field behavior. For skin-thick films, the sharp subwavelength behavior leads to a strong Fabry-Perot enhancement of the total transmittance, and of light inside the slit. Oblique incidence strongly facilitates the excitation of the nonzero eigenmodes leading to mode competition. Only few selectively excited modes are strongly involved in the near-subwavelength transmission/diffraction phenomena. The results obtained can serve as a reference point in subwavelength optics of real metals.

ACKNOWLEDGMENTS

Financial support from the Programs of Presidium RAN 21.2 and BPS of RAN "Physics of new materials and structures" is acknowledged.

[1] L. Rayleigh, Proc. R. Soc. London, Ser. A **89**, 194 (1913); Philos. Mag. **14**, 60 (1907).
[2] A. Sommerfeld, *Optics* (Academic Press, New York, 1954).
[3] H. A. Bethe, Phys. Rev. **66**, 163 (1944).
[4] C. J. Bouwkamp, Rep. Prog. Phys. **17**, 35 (1954).
[5] L. D. Landau and E. M. Lifshits, *Electrodynamics of continuous media* (Pergamon Press, Oxford, 1984).
[6] J. Meixner, IEEE Trans. Antennas Propag. **20**, 442 (1972).
[7] E. Betzig and J. K. Trautman, Science **257**, 189 (1992).
[8] M. T. Hill, Y. Oei, B. Smalbrugge, Y. Zhu, T. de Vries, P. J. van Veldhoven, F. W. M. van Otten, T. J. Eijkemans, J. P. Turkiewicz, H. de Waardt, E. J. Geluk, S.-H. Kwon, Y.-H. Lee, R. Nötzel, and M. K. Smit, Nat. Photonics **1**, 589 (2007).
[9] J. N. Anker, W. P. Hall, O. Lyandres, N. C. Shah, J. Zhao, and R. P. Van Duyne, Nature Mater. **7**, 442 (2008).
[10] T. W. Ebbesen, H. J. Lezec, H. F. Ghaemi, T. Thio, and P. A. Wolff, Nature (London) **391**, 667 (1998).
[11] C. Genet and T. W. Ebbesen, Nature (London) **445**, 39 (2007).
[12] W. L. Barnes, A. Dereux, and T. W. Ebbesen, Nature (London) **424**, 824 (2003).
[13] F. J. García-Vidal and L. Martín-Moreno, Phys. Rev. B **66**, 155412 (2002).
[14] H. Liu and Ph. Lalanne, Nature (London) **452**, 728 (2008).
[15] B. Sturman, E. Podivilov, and M. Gorkunov, Phys. Rev. B **77**, 075106 (2008).
[16] J. D. Jackson, *Classical Electrodynamics* (Wiley, New York, 1998).
[17] A. Roberts, J. Opt. Soc. Am. A **4**, 1970 (1987).
[18] L. Novotny and C. Hafner, Phys. Rev. E **50**, 4094 (1994).
[19] H. M. Nussenzveig, Philos. Trans. R. Soc. London **252**, 31 (1959).
[20] Y. Takakura, Phys. Rev. Lett. **86**, 5601 (2001).
[21] F. Yang and J. R. Sambles, Phys. Rev. Lett. **89**, 063901 (2002).
[22] H. F. Schouten, T. D. Visser, D. Lenstra, and H. Blok, Phys. Rev. E **67**, 036608 (2003).
[23] H. F. Schouten, T. D. Visser, G. Gbur, D. Lenstra, and H. Blok, Phys. Rev. Lett. **93**, 173901 (2004).
[24] J. Bravo-Abad, L. Martin-Moreno, and F. J. Garcia-Vidal, Phys. Rev. E **69**, 026601 (2004).
[25] Ph. Lalanne, J. P. Hugonin, and J. C. Rodier, Phys. Rev. Lett. **95**, 263902 (2005).
[26] P. Lalanne, J. P. Hugonin, and J. C. Rodier, J. Opt. Soc. Am. B **23**, 1608 (2006).
[27] H. F. Schouten, N. Kuzmin, G. Dubois, T. D. Visser, G. Gbur, P. F. Alkemade, H. Blok, G. W. 't Hooft, D. Lenstra, and E. R. Eliel, Phys. Rev. Lett. **94**, 053901 (2005).
[28] G. Gay, O. Alloschery, B. Viaris de Lesegno, J. Weiner, and H. J. Lezec, Phys. Rev. Lett. **96**, 213901 (2006).
[29] A. I. Fernández-Domínguez, F. J. García-Vidal, and L. Martín-Moreno, Phys. Rev. B **76**, 235430 (2007).
[30] H. Bateman and A. Erdelyu, *Higher Transcendental Functions II* (Mc Graw-Hill, New York, 1953).
[31] R. Gordon, Phys. Rev. B **73**, 153405 (2006).
[32] B. Sturman, E. Podivilov, and M. Gorkunov, Phys. Rev. B **76**, 125104 (2007).
[33] *Handbook of Optics*, edited by M. Bass (McGraw-Hill, New York, 1995), Vol. 2.